Optical mode conversion through nonlinear two-wave mixing

D. G. Pires, J. C. A. Rocha, A. J. Jesus-Silva, and E. J. S. Fonseca*
Optics and Nanoscopy Group, Universidade Federal de Alagoas, 57061-670, Maceió, AL, Brazil

(Received 3 May 2019; published 14 October 2019)

Hermite-Gaussian (HG), Laguerre-Gaussian (LG), and Ince-Gaussian (IG) modes have been of considerable importance for photonics. They have revealed a unique way to optical manipulation and are particularly promising for optical communications. This paper combines HG modes, as a basis, inside the nonlinear crystal and the generated second harmonic field turns to LG and IG modes. Here we present a way to use second order nonlinear media to convert optical beam modes as we wish.

DOI: 10.1103/PhysRevA.100.043819

I. INTRODUCTION

Undoubtedly, photonics achieved a great position in the present scientific picture. Among the many applications it has led us to, the enhancements in the communication system and optical micromanipulation are the most highlighted ones. Spatially structured light, which can be defined as a bidimensional design of the transverse higher-order light modes, is one of the ways to code information or be used in optical tweezers and trapping. The potential of higher order spatial light modes with defined, complex propagation properties, such as the Hermite-Gaussian (HG), Laguerre-Gaussian (LG), and, recently, Ince-Gaussian (IG) modes, has attracted steady attention of researchers over the last decades. Particularly, LG modes are of highest interest in optical micromanipulation [1] and communication [2]. Since its discovery [3], many studies on fundamental properties [4,5], optical tweezers [6], spin-orbit coupling [7], teleportation schemes [8,9], imaging [10], manipulation of ultracold atoms [11], and quantum protocols [12,13] to cite a few, were realized.

On other hand, nonlinear responses can be useful in order to mediate some photonic processes. Nonlinear media can bring very interesting effects like second harmonic generation [14] and sum-difference frequency generation [15], optical parametric oscillation [16], parametric fluorescence [17], nonlinear mixing [18,19], and four-wave mixing in atomic media [20,21]. The beam coupling due to two-wave mixing has been studied [22–24], showing how optical vortices behave in the second harmonic generation (SHG). The nonlinear media acts like a mode selector, leading to mode superposition in the second harmonic field. This effect happens when the wave mixing is under longitudinal and transversal phase match, and this role is played by the overlap integral within the nonlinear media.

Optical mode conversion is mainly realized by using diffractive and linear optics [25–27]. Here we present a way to use second order nonlinear media to convert optical beam modes as we wish. It is well known that HG and LG are transversal eigenmodes of typical laser resonators and can easily be created with high efficiency [28,29]. These two modes separately form two complete families of exact and orthogonal solutions of the paraxial wave equation (PWE) in rectangular and cylindrical coordinates, respectively. More recently, IG modes have been proposed as a third complete family of PWE solutions in elliptic coordinates [30]. By using HG modes as a basis, we combine multiple beams inside the nonlinear crystal and the generated second harmonic field turns as a combination of HG modes, leading to the conversion into LG and IG modes. In order to better visualize the mode decomposition, Fig. 1(a) shows a Poincaré sphere for a set of mode conversions in a particular HG basis. Modal conversion and decomposition of HG modes in the spatial-temporal degree of freedom were considered before for tailoring its temporal-mode structures [31–34]. The results presented here, together with previous works on spatial-temporal control of structured beams [35,36], are important for communication systems.

II. NONLINEAR TWO-WAVE MIXING OF HERMITE-GAUSSIAN BEAMS

In the paraxial approximation, the second harmonic generation under longitudinal and transversal phase match conditions is described by a coupled evolution for the incoming fields U_h and U_v, orthogonally polarized in respect of each other and frequency ω, generating a field $U_{2\omega}$ [24,37]. The expansion of these fields in an orthonormal basis is [24]

$$U_j = \sqrt{\frac{\omega_j}{n_j}} \sum_{m,n} A^j_{mn} u^j_{mn}(\mathbf{r}, z), \tag{1}$$

where n_j is the refractive index for the U_j field, u^j_{mn} is the mode basis, and A^j_{mn} is the amplitude with $j = h, v, 2\omega$. Although the basis of the expansion is arbitrary, it must be chosen carefully. In our case, the bases used are the HG modes. Figure 1(c) shows a sketch of the nonlinear two-wave mixing process considered here. Notice that the generated field $U_{2\omega}$ is a sum-frequency field but, since its frequency is 2ω and for convention reasons, we will call $U_{2\omega}$ as a second harmonic generated field.

*efonseca@fis.ufal.br

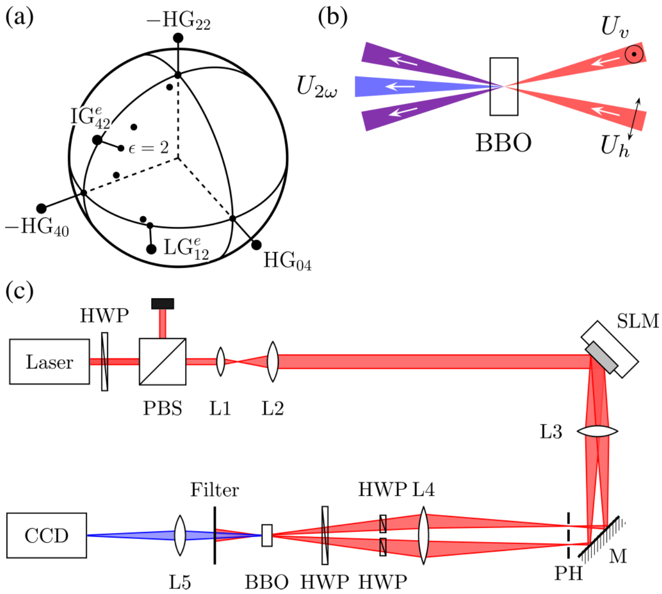

FIG. 1. (a) Three-dimensional graphical representation of IG^e_{42} mode with various eccentricity values expanded in the HG mode basis. (b) General idea of the nonlinear two-wave mixing process. (c) Sketch of the experimental setup. HWP: half-wave plate; PBS: polarized beam splitter; SLM: spatial light modulator; L: lens; PH: pinhole; BBO: beta barium borate; CCD: coupled-charged device.

After this mode decomposition, the coupled equations for the amplitudes can be written as [24]

$$\begin{aligned}
\frac{dA^h_{mn}}{dz} &= ig\sum_{m'n'}\sum_{m''n''}\Lambda^{n'nn''}_{m'mm''}A^{2\omega}_{m'n'}\left(A^v_{m''n''}\right)^*,\\
\frac{dA^v_{mn}}{dz} &= ig\sum_{m'n'}\sum_{m''n''}\Lambda^{n'n''n}_{m'm''m}A^{2\omega}_{m'n'}\left(A^h_{m''n''}\right)^*,\\
\frac{dA^{2\omega}_{mn}}{dz} &= ig\sum_{m'n'}\sum_{m''n''}\left(\Lambda^{nn'n''}_{mm'm''}\right)^*A^h_{m'n'}A^v_{m''n''}.
\end{aligned} \tag{2}$$

Here we consider $\chi = \chi^*$ and $\Lambda^{ll'l''}_{pp'p''} = (\Lambda^{ll'l''}_{pp'p''})^*$ by neglecting nonlinear losses and the Gouy phase acquired inside the crystal, respectively. The introduced parameters are [24]

$$\begin{aligned}
R^{nn'n''}_{mm'm''} &= \int u^{2\omega}_{mn}\left(u^h_{m'n'}\right)^*\left(u^v_{m''n''}\right)^* d^2\mathbf{r},\\
\Lambda^{nn'n''}_{mm'm''} &= \frac{R^{nn'n''}_{mm'm''}}{R^{000}_{000}},\\
g &= \frac{\chi}{2c}\sqrt{\frac{2\omega^3}{n_h n_v n_{2\omega}}}R^{000}_{000}.
\end{aligned} \tag{3}$$

The overlap integral $\Lambda^{nn'n''}_{mm'm''}$ plays the main role in the mode conversion acting as a mode selector for the mixed fields inside the nonlinear crystal. For HG modes, the normalized overlap integral is [38]

$$\begin{aligned}
\Lambda^{nn'n''}_{mm'm''} = \Lambda^{000}_{000}C^{nn'n''}_{mm'm''}&\frac{\partial^{m'+m''}}{\partial t_1^{m'}\partial t_2^{m''}}\left[(t_1+t_2)^m e^{-(t_1+t_2)^2/2}\right]\Big|_{t_i=0}\\
\times&\frac{\partial^{n'+n''}}{\partial t_1^{n'}\partial t_2^{n''}}\left[(t_1+t_2)^n e^{-(t_1+t_2)^2/2}\right]\Big|_{t_i=0},
\end{aligned} \tag{4}$$

where $C^{nn'n''}_{mm'm''} = \sqrt{\frac{2^{-(m+m'+m''+n+n'+n'')}}{m!m'!m''!n!n'!n''!}}$ and Λ^{000}_{000} is a normalizing constant. An interesting effect is worth noting here. For HG mode mixtures, the second harmonic generated field has a single mode with indexes equal to $m = m' + m''$ and $n = n' + n''$, not a superposition of modes with $m \leqslant m' + m''$ and $n \leqslant n' + n''$ observed in the LG mode mixing. All the lower orders in the expansion vanish due to the overlap integral acquiring undetermined values, remaining only a higher order term. This is not an intuitive effect, since for a Laguerre-Gaussian (LG) mode mixture the generated field is a superposition of different radial modes [23] and will be better treated in a coming work. For this reason, HG modes form a unique basis for this purpose, since for an efficient conversion we must make sure that a specific mode will be created.

Now, instead of using a single mode as input beam, a combination of HG with different indexes is considered. This means that, from now on, $U_h = \sum_{mn}\alpha_{mn}\mathrm{HG}_{mn}$ and $U_v = \sum_{mn}\beta_{mn}\mathrm{HG}_{mn}$, where α_{mn} and β_{mn} are the weights of each mode in the sum and, physically, can be understood as intensity control parameters. Notice that after performing the overlap integral, we have a sum of normalized overlaps

$$\Lambda_{\mathrm{Net}} = \sum_i \Lambda_i, \tag{5}$$

where each Λ_i must select the HG mode superposition in the second harmonic field. By choosing these modes properly, it is possible to convert them into different kind of modes, such as IG or LG modes. The basis is chosen by expanding IG and LG modes in terms of HG ones [30]. The SHG process is illustrated in Fig. 1(b) which shows two orthogonally polarized beams, U_h and U_v. In each beam we have a superposition of HG modes, going through a process of nonlinear mixture inside the BBO crystal and generating the desired IG or LG mode in the second harmonic field $U_{2\omega}$. A detailed look on how the weights are chosen can be found in Appendix A.

III. BEAMS WITH DEFINED PARITY

Theoretical calculations, along with experimental validation, were performed. When the Rayleigh length is much larger than the size of the nonlinear crystal, the coupled equations for the amplitude evolution in Eq. (2) can be simplified and analytically solved [16]. Here the Rayleigh length is around 20 cm. The resulting second harmonic field, which is composed by a superposition of HG modes, is then calculated at the Fraunhofer zone.

Figure 1(c) shows a sketch of the experimental setup. A pulsed Ti:sapphire laser tuned at 780 nm illuminates a spatial light modulator (SLM), generating two HG superposition beams with a linear phase difference. A computer-generated double-phase hologram [39,40] is used to encode the resulting field. After the beams are separated, each one passes through a half-wave plate (HWP) in order to set an orthogonally polarization in respect of each other, then another HWP is used to obtain a most efficient SHG from a type II beta barium borate (BBO) nonlinear crystal with size 10 × 10 × 3 mm and phase-matching angle $\theta = 33.5^\circ$. After the beam of interest is generated, a spectral filter separates it from the near infrared beams and its far field intensity pattern is captured by

TABLE I. Input beams decomposition in HG basis that generates a specified IG or LG mode through a nonlinear two-wave mixing process. Modes marked with $*$ denotes those in which it is not possible to find a solution for linear system for the weights ($\alpha_{m'n'}$ and $\beta_{m''n''}$) that compensates the overlap integral $\Lambda^{nn'n''}_{mm'm''}$ that arises from the selection rule.

Mode	U_h	U_v
IG^e_{22}	$HG_{10} + 0.486HG_{01}$	$3.892HG_{10} - 1.892HG_{01}$
IG^e_{42}	$HG_{20} - 0.155HG_{02}$	$-12.000HG_{20} - 25.843HG_{02}$
IG^o_{31}	$2.072HG_{20} + 4.462HG_{02}$	HG_{01}
LG^e_{01}	$HG_{10}+HG_{01}$	$HG_{10} - HG_{01}$
LG^e_{12}	$HG_{20}+HG_{02}$	$HG_{20} - HG_{02}$
LG^o_{11}	$HG_{20}+HG_{02}$	HG_{01}
LG_{02}	$HG_{10} - 1.017iHG_{01}$	$-2.828HG_{10}+2.779iHG_{01}$
$^*LG_{12}$	$HG_{20}+HG_{02}$	$HG_{20} - HG_{02} - iHG_{02}$
IG_{22}	$HG_{10} - 1.267iHG_{01}$	$-3.892HG_{10}+0.726iHG_{01}$
$^*IG_{31}$	$2.859HG_{20}+0.983HG_{02}$	$1.577iHG_{10}+2.405HG_{01}$

a coupled-charged device (CCD) camera. An interesting fact about using this setup is that it assures both beams have the same optical path, implying no need for a translation stage to temporally match the pulses. It becomes much easier to conduct these kinds of experiments.

The input beams must be chosen properly in each branch U_h and U_v. For example, for the $IG^e_{2,2}$ mode we need to expand

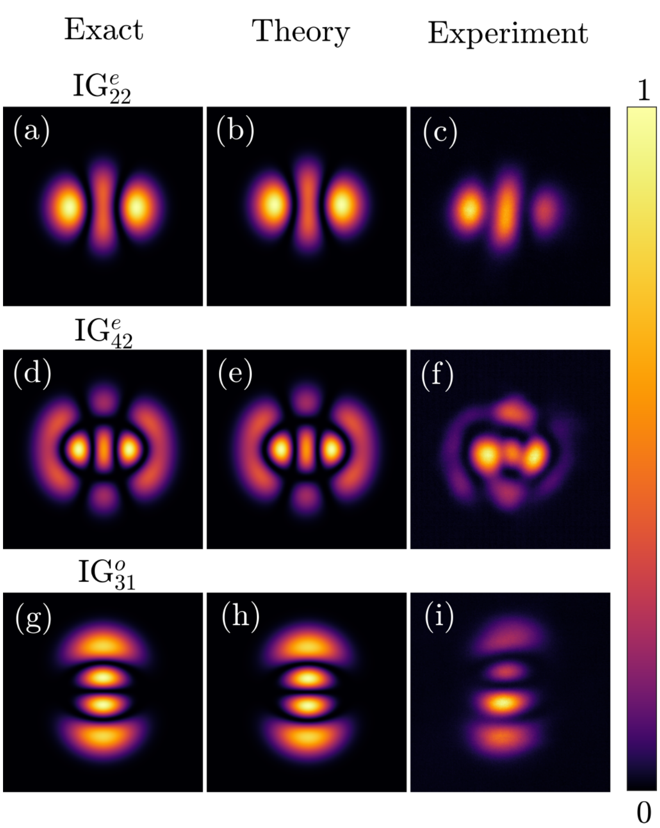

FIG. 2. Exact IG mode (a), (d), and (g) compared with the theoretical (b), (e), and (h) and experimental (c), (f), and (i) intensity patterns for even and odd parities.

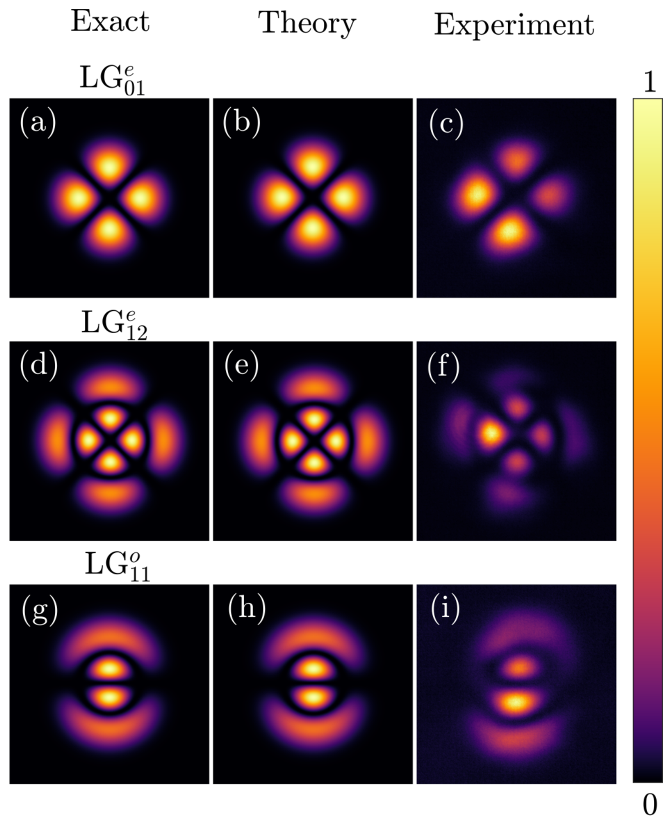

FIG. 3. Exact LG mode (a), (d), and (g) compared with the theoretical (b), (e), and (h) and experimental (c), (f), and (i) intensity patterns for even and odd parities.

it in terms of the modes HG_{20} and HG_{02}. But, in order to generate a combination of these modes in the second harmonic beam, we must use

$$U_h = \alpha_{10}HG_{10} + \alpha_{01}HG_{01} \tag{6}$$

and

$$U_v = \beta_{10}HG_{10} + \beta_{01}HG_{01}. \tag{7}$$

Here the values for $\alpha_{m'n'}$ and $\beta_{m''n''}$ are determined by combining the beams in Eqs. (6) and (7) as shown in Table I. The normalized overlap integral $\Lambda^{nn'n''}_{mm'm''}$ is the one responsible for mixing the input modes, creating the field superposition in the second harmonic beam. Therefore, we need to compensate its values while choosing the weights $\alpha_{m'n'}$ and $\beta_{m''n''}$. The expansions for the other modes studied in this paper are also displayed in Table I.

First, we selected a group of three different modes with well-defined beam parities. The results for the IG and LG conversions can be seen in Figs. 2 and 3, respectively, following the first to seventh line of Table I. The first column shows the exact intensity distribution for the desired IG and LG modes, obtained as solutions for the paraxial wave equation in an elliptical coordinate system. Expressions for the exact transverse field can be found in Ref. [30]. The second column shows theoretical results which represent the second harmonic field calculated using the normalized overlap expression in Eq. (4) for HG beams in the nonlinear mixture and then propagated until the Fraunhofer zone. The third column shows

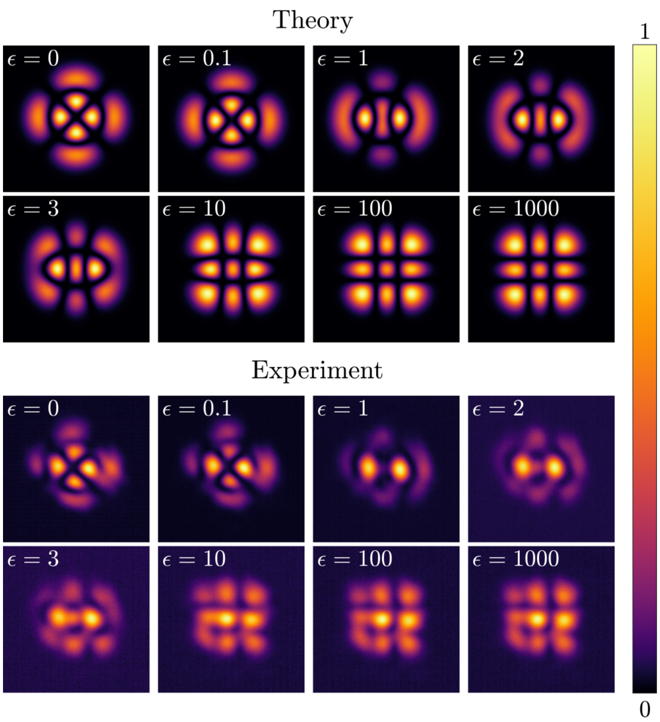

FIG. 4. Far field second harmonic intensity distribution for various eccentricity values of the IG^e_{42} mode. Here we show the transition between LG and HG modes by changing the eccentricity from 0 to 1000.

the experimental results to validate our theory. The weights α_{mn} and β_{mn} were calculated by considering the expansion of the IG and LG modes in the HG basis [41] and taking into account the value of the normalized overlap $\Lambda^{nn'n''}_{mm'm''}$, leading to a set of equations that can be easily solved (see Table I). As a helpful visualization sketch, the Poincaré sphere in Fig. 1(b) can be used for a better understanding of the mode transformations. These points were also considered for the computer generated holograms used in the experimental results. The weights values for the input beams were inserted in the hologram expression already anticipating the usual normalized overlap weight acquired by each beam in the nonlinear mixture. By means of a convex lens (L5), the generated second harmonic beams were propagated until the Fourier plane, where their intensity profiles were captured and can be seen in the experiment column of Figs. 2 and 3. Additionally, we show the transition between LG and HG modes by changing the eccentricity parameter of a IG^e_{42} mode. Figure 4 shows the intensity distributions of the second harmonic generated beam at the Fraunhofer zone, theoretically and experimentally, for eccentricity values between 0 and 1000. Here we can always find a set of weights so that the output SHG field will have the exact decomposition of the desired mode in HG basis. Although the similarities between the theoretical and experimental results compared with the exact transverse field distribution are remarkable, we can note a shear in the measured intensity patterns. A slightly spatial-temporal mismatch at the nonlinear crystal may occur, where such experimental error leads to an imperfect intensity distribution.

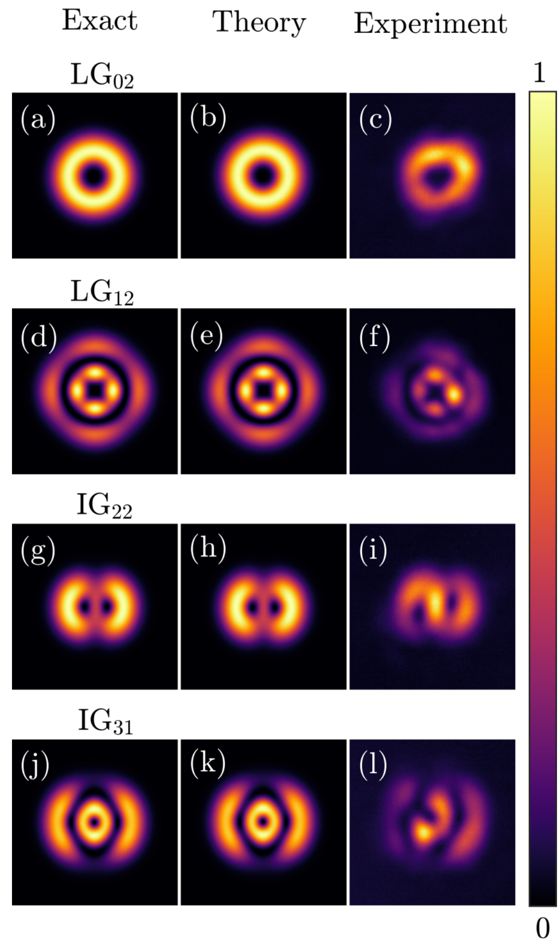

FIG. 5. Exact LG (a) and (d) and IG (g) and (j) modes compared with the theoretical (b), (e), (h), and (k) and experimental (c), (f), (i), and (l) intensity patterns for beams carrying OAM.

IV. BEAMS CARRYING ORBITAL ANGULAR MOMENTUM

As we are converting HG beams into LG beams with well-defined parity, they do not possess OAM. In order to generate a beam carrying a specific topological charge, the superposition in the second harmonic field must combine beams with even and odd parities. Figure 5 shows a set of IG and LG beams generated by the combination of HG modes that carries OAM. In this case, we must add a $e^{i\pi/2}$ phase to one of the mode parities in order to access a specific point in the Poincaré sphere. The last four lines of Table I show the mode superposition used with its weight value, to generate beams carrying OAM in SHG. Note that, for instance, the theoretical and experimental results for the LG_{12} do not match perfectly its exact transverse field mode. In this case, the set of equations for the weight values cannot be solved exactly. Although the intensity profile cannot be obtained precisely as it should be, in fact the results in Fig. 5 possess OAM (see Appendix B for more details on the limitations of the presented method). In order to prove that, we measure the topological charge by using the tilted-lens method [42] for the second harmonic generated beams presented in Fig. 5. In Fig. 6 we show the intensity distributions for the considered

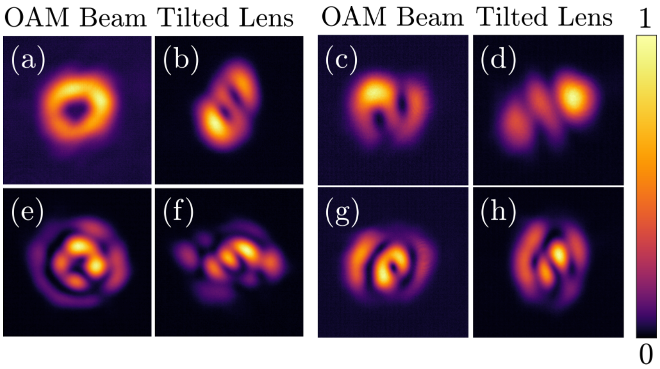

FIG. 6. Far field second harmonic intensity distribution for beams possessing OAM referring to the modes (a) $^*\mathrm{LG}_{02}$, (c) LG_{12}, (e) IG_{22}, and (g) $^*\mathrm{IG}_{31}$, together with the associated topological charge measure performed using the tilted-lens method (b), (d), (f), and (h), respectively. Modes marked with $*$ denotes those in which it is not possible to find a solution for linear system for the weights ($\alpha_{m'n'}$ and $\beta_{m''n''}$) that compensates the overlap integral $\Lambda_{mm'm''}^{nn'n''}$ that arises from the selection rule.

beams, where the topological charge is equal to the number of maxima minus one.

V. CONCLUSIONS

In summary, by means of a theoretical and experimental approach, we present an alternative way of using nonlinear two-wave mixing to convert HG modes into IG and LG modes. When multiple modes are used as input beams, the selection rule played by the normalized overlap integral selects the needed modes which will be converted into new modes possessing different symmetry. Results for beams with well-defined parity and carrying OAM were generated. Our paper could be helpful for designing new types of modes, where the beam shape could be selected by the user, implying new ways to optical manipulation as well as promising for optical communications.

ACKNOWLEDGMENTS

This study was financed in part by Coordenação de Aperfeiçoamento de Pessoal e Nível Superior—Brasil (CAPES)—Finance Code 001, Conselho Nacional de Desenvolvimento Científico e Tecnológico (CNPq), Fundação de Amparo à Pesquisa do Estado de Alagoas (FAPEAL), and Instituto Nacional de Ciência e Tecnologia de Informação Quântica (INCT-IQ).

APPENDIX A: MODE DECOMPOSITION

Let us consider each parity separately. The first step is to expand the desired mode into the HG basis [30,41]. As an example for odd parities, let us use the IG_{31}^o for the following explanation. This mode can be expanded in terms of HG modes as

$$\mathrm{IG}_{31}^o = A\mathrm{HG}_{21} + B\mathrm{HG}_{03} \tag{A1}$$

with constants A and B depending on the eccentricity of the beam. Now we need to choose the combination of HG modes as input beams in order to result in the above modes after the second harmonic generation (SHG). For example, if we want to generate the mode HG_{mn} we must use $\mathrm{HG}_{m'n'}$ and $\mathrm{HG}_{m''n''}$ as input modes U_h and U_v on any order. Following this idea, one possible configuration can be

$$\begin{aligned} U_h &= \alpha_{20}\mathrm{HG}_{20} + \alpha_{02}\mathrm{HG}_{02},\\ U_v &= \beta_{01}\mathrm{HG}_{01}, \end{aligned} \tag{A2}$$

where α_{20}, α_{02}, and β_{01} constants must be determined. Notice that these constants can be seen as intensity control parameters. Using the above expressions and following the steps of the main article, the SHG field, carrying the overlap integral constant, is

$$U_{2\omega} = \alpha_{20}\beta_{01}\Lambda_{220}^{101}\mathrm{HG}_{21} + \alpha_{02}\beta_{01}\Lambda_{000}^{321}\mathrm{HG}_{03}. \tag{A3}$$

Since we want the generated field to be the one from Eq. (1), we must adjust α_{20}, α_{02}, and β_{01} for that purpose. This forms a linear system to be solved for those constants

$$\begin{aligned} \alpha_{20}\beta_{01}\Lambda_{220}^{101} &= A,\\ \alpha_{02}\beta_{01}\Lambda_{000}^{321} &= B, \end{aligned} \tag{A4}$$

with one possible solution being

$$\alpha_{20} = \frac{A}{\Lambda_{220}^{101}}, \quad \alpha_{02} = \frac{B}{\Lambda_{000}^{321}}, \quad \beta_{01} = 1. \tag{A5}$$

This method can be generalized for any mode with odd parity written in the HG basis:

$$\mathrm{IG}_{pm}^o = \sum_{m'n'} \alpha_{m'n'}\mathrm{HG}_{m'n'}, \tag{A6}$$

with input beams

$$U_h = \sum_{m''n''} \beta_{m''n''}\mathrm{HG}_{m''n''}, \tag{A7}$$

$$U_v = \mathrm{HG}_{01} \quad \text{or} \quad U_v = \mathrm{HG}_{10}, \tag{A8}$$

and weights

$$\beta_{m''n''} = \frac{\alpha_{m'n'}}{\Lambda_{mm'm''}^{nn'n''}}. \tag{A9}$$

For modes with even parity, we use IG_{42}^e as an example. It is written in the HG basis as

$$\mathrm{IG}_{42}^e = A\mathrm{HG}_{40} + B\mathrm{HG}_{22} + C\mathrm{HG}_{04}. \tag{A10}$$

In this case, we can decompose the input beams as follows:

$$\begin{aligned} U_h &= \alpha_{20}\mathrm{HG}_{20} + \alpha_{02}\mathrm{HG}_{02},\\ U_v &= \beta_{20}\mathrm{HG}_{20} + \beta_{02}\mathrm{HG}_{02}, \end{aligned} \tag{A11}$$

with α_{20},α_{02},β_{20}, and β_{02} constants to be determined. Using those input beams, the SGH field takes the form

$$\begin{aligned} U_{2\omega} = {}& \alpha_{20}\beta_{20}\Lambda_{422}^{000}\mathrm{HG}_{40} + \alpha_{20}\beta_{02}\Lambda_{220}^{202}\mathrm{HG}_{22}\\ &+ \alpha_{02}\beta_{20}\Lambda_{202}^{220}\mathrm{HG}_{22} + \alpha_{02}\beta_{02}\Lambda_{000}^{422}\mathrm{HG}_{04}. \end{aligned} \tag{A12}$$

We can group the HG_{22} terms since $\Lambda^{202}_{220} = \Lambda^{220}_{202}$, and thus we have

$$U_{2\omega} = \alpha_{20}\beta_{20}\Lambda^{000}_{422}HG_{40} + (\alpha_{20}\beta_{02} + \alpha_{02}\beta_{20})\Lambda^{202}_{220}HG_{22} + \alpha_{02}\beta_{02}\Lambda^{422}_{000}HG_{04}. \tag{A13}$$

This leads to the following linear system:

$$\begin{aligned} \alpha_{20}\beta_{20}\Lambda^{000}_{422} &= A,\\ (\alpha_{20}\beta_{02} + \alpha_{02}\beta_{20})\Lambda^{202}_{220} &= B,\\ \alpha_{02}\beta_{02}\Lambda^{422}_{000} &= C. \end{aligned} \tag{A14}$$

One possible solution is given by

$$\alpha_{20} = 1, \quad \alpha_{02} = \frac{B/\Lambda^{202}_{220} \pm \sqrt{(B/\Lambda^{202}_{220})^2 - 4AC/\Lambda^{202}_{220}\Lambda^{422}_{000}}}{2A/\Lambda^{000}_{422}},$$
$$\beta_{20} = \frac{A}{\alpha_{20}\Lambda^{000}_{422}}, \quad \beta_{02} = \frac{C}{\alpha_{02}\Lambda^{422}_{000}}. \tag{A15}$$

APPENDIX B: LIMITATIONS OF THE METHOD

Differently than odd parity modes, we cannot always find a nontrivial combination for the input beams in which the SGH field is the desired mode. In those cases, the linear system to be solved for the weights is inconsistent, and thus a solution is not available. Take for example IG^e_{62}:

$$IG^e_{62} = AHG_{60} + BHG_{42} + CHG_{24} + DHG_{06}, \tag{B1}$$

which is decomposed in the input beams

$$\begin{aligned} U_h &= \alpha_{40}HG_{40} + \alpha_{04}HG_{04},\\ U_v &= \beta_{20}HG_{20} + \beta_{02}HG_{02}. \end{aligned} \tag{B2}$$

The linear system for the weights takes the form

$$\begin{aligned} \alpha_{40}\beta_{20}\Lambda^{000}_{642} &= A,\\ \alpha_{40}\beta_{02}\Lambda^{202}_{440} &= B,\\ \alpha_{04}\beta_{20}\Lambda^{440}_{202} &= C,\\ \alpha_{04}\beta_{02}\Lambda^{642}_{000} &= D, \end{aligned} \tag{B3}$$

which is inconsistent and does not have a solution.

A similar behavior occurs with OAM carrying beams. As for demonstration of this limitation let us consider the LG_{12} mode which decomposes in HG basis as follows:

$$LG_{12} = LG^e_{12} + iLG^o_{12} = HG_{40} - HG_{04} + i(HG_{31} + HG_{13}), \tag{B4}$$

with all different multiplicative constants, as in the previous IG^e_{62} case. This means that we will end up with a similar inconsistent linear system for the weights. Even though, in this case, we cannot generate the exact LG_{12} mode, it is possible to find a decomposition for the incoming beams U_v and U_h that $U_{2\omega}$ will possess OAM, as demonstrated Figs. 2(c), 2(f), 2(g), and 2(h).

In the case of Fig. 2(c) we use the following superposition:

$$\begin{aligned} U_h &= HG_{20} - HG_{02} - iHG_{11},\\ U_v &= HG_{20} + HG_{02}. \end{aligned} \tag{B5}$$

The SHG field $U_{2\omega}$ takes the form

$$U_{2\omega} = \Lambda^{000}_{422}HG_{40} + \Lambda^{202}_{220}HG_{22} - \Lambda^{220}_{202}HG_{22} - \Lambda^{422}_{000}HG_{04} - i\Lambda^{110}_{312}HG_{31} - i\Lambda^{312}_{110}HG_{13}. \tag{B6}$$

Notice that if all $\Lambda^{nn'n''}_{mm'm''}$ were equal, we would have $U_{2\omega} = LG_{12}$ up to some proportionality constant. Since they are not the same, the overlap integral imposes different weights to the HG modes than those which would have generated the exact LG_{12} mode. Regardless of this variation, $U_{2\omega}$ transverse intensity pattern still resembles the LG_{12} mode and carry optical singularities, as can be seen in Figs. 2(e) and 2(f).

On the other hand, even if we cannot find appropriate weights to compensate the overlap integral, it is possible to numerically optimize them using various minimum search methods for multivariable functions [43,44]. In our case, we are trying to find weights $\alpha_{m'n'}$ and $\beta_{m''n''}$ such that the resulting second harmonic field $U_{2\omega}$ approximate the desired IG mode with specified eccentricity ε and parity σ, IG^σ_{pm}. This is achieved by minimizing the quantity $\sum_{i,j}|U_{2\omega} - IG^\sigma_{pm}|^2$ where the indices i and j goes through all sampled points of the discretized fields. The result of this process is depicted in Figs. 5(g) and 5(h) which shows that the optimized solution still possess OAM.

[1] M. Woerdemann, C. Alpmann, M. Esseling, and C. Denz, Advanced optical trapping by complex beam shaping, Laser Photon. Rev. **7**, 839 (2013).

[2] A. E. Willner, H. Huang, Y. Yan, Y. Ren, N. Ahmed, G. Xie, C. Bao, L. Li, Y. Cao, Z. Zhao, J. Wang, M. P. J. Lavery, M. Tur, S. Ramachandran, A. F. Molisch, N. Ashrafi, and S. Ashrafi, Optical communications using orbital angular momentum beams, Adv. Opt. Photon. **7**, 66 (2015).

[3] L. Allen, M. W. Beijersbergen, R. Spreeuw, and J. Woerdman, Orbital angular momentum of light and the transformation of Laguerre-Gaussian laser modes, Phys. Rev. A **45**, 8185 (1992).

[4] A. M. Yao and M. J. Padgett, Orbital angular momentum: Origins, behavior and applications, Adv. Opt. Photon. **3**, 161 (2011).

[5] J. M. Hickmann, E. J. S. Fonseca, and A. J. Jesus-Silva, Born's rule and the interference of photons with orbital angular momentum by a triangular slit, Europhys. Lett. **96**, 64006 (2011).

[6] M. Padgett and R. Bowman, Tweezers with a twist, Nat. Photon. **5**, 343 (2011).

[7] X. Y. Xiong, A. Al-Jarro, L. J. Jiang, N. C. Panoiu, and E. Wei, Mixing of spin and orbital angular momenta via second-harmonic generation in plasmonic and dielectric chiral nanostructures, Phys. Rev. B **95**, 165432 (2017).

[8] L. Chen and W. She, Teleportation of a controllable orbital angular momentum generator, Phys. Rev. A **80**, 063831 (2009).

[9] J. T. Barreiro, T.-C. Wei, and P. G. Kwiat, Remote Preparation of Single-Photon "Hybrid" Entangled and Vector-Polarization States, Phys. Rev. Lett. **105**, 030407 (2010).

[10] C. Maurer, A. Jesacher, S. Bernet, and M. Ritsch-Marte, What spatial light modulators can do for optical microscopy, Laser Photon. Rev. **5**, 81 (2011).
[11] V. Galitski and I. B. Spielman, Spin–orbit coupling in quantum gases, Nature (London) **494**, 49 (2013).
[12] L. Aolita and S. Walborn, Quantum Communication without Alignment Using Multiple-Qubit Single-Photon States, Phys. Rev. Lett. **98**, 100501 (2007).
[13] V. D'ambrosio, E. Nagali, S. P. Walborn, L. Aolita, S. Slussarenko, L. Marrucci, and F. Sciarrino, Complete experimental toolbox for alignment-free quantum communication, Nat. Commun. **3**, 961 (2012).
[14] K. Dholakia, N. Simpson, M. Padgett, and L. Allen, Second-harmonic generation and the orbital angular momentum of light, Phys. Rev. A **54**, R3742 (1996).
[15] A. Berzanskis, A. Matijosius, A. Piskarskas, V. Smilgevicius, and A. Stabinis, Conversion of topological charge of optical vortices in a parametric frequency converter, Opt. Commun. **140**, 273 (1997).
[16] C. Schwob, P.-F. Cohadon, C. Fabre, M. Marte, H. Ritsch, A. Gatti, and L. Lugiato, Transverse effects and mode couplings in OPOs, Appl. Phys. B **66**, 685 (1998).
[17] E. Nagali and F. Sciarrino, Generation of hybrid polarization-orbital angular momentum entangled states, Opt. Express **18**, 18243 (2010).
[18] A. Bahabad and A. Arie, Generation of optical vortex beams by nonlinearwave mixing, Opt. Express **15**, 17619 (2007).
[19] T. Roger, J. J. Heitz, E. M. Wright, and D. Faccio, Non-collinear interaction of photons with orbital angular momentum, Sci. Rep. **3**, 3491 (2013).
[20] J. Tabosa and D. Petrov, Optical Pumping of Orbital Angular Momentum of Light in Cold Cesium Atoms, Phys. Rev. Lett. **83**, 4967 (1999).
[21] S. Barreiro and J. Tabosa, Generation of Light Carrying Orbital Angular Momentum via Induced Coherence Grating in Cold toms, Phys. Rev. Lett. **90**, 133001 (2003).
[22] W. Buono, J. Santiago, L. Pereira, D. Tasca, K. Dechoum, and A. Khoury, Polarization-controlled orbital angular momentum switching in nonlinear wave mixing, Opt. Lett. **43**, 1439 (2018).
[23] L. J. Pereira, W. T. Buono, D. S. Tasca, K. Dechoum, and A. Z. Khoury, Orbital-angular-momentum mixing in type-II second-harmonic generation, Phys. Rev. A **96**, 053856 (2017).
[24] W. Buono, L. Moraes, J. Huguenin, C. Souza, and A. Khoury, Arbitrary orbital angular momentum addition in second harmonic generation, New J. Phys. **16**, 093041 (2014).
[25] A. T. O'Neil and J. Courtial, Mode transformations in terms of the constituent Hermite–Gaussian or Laguerre–Gaussian modes and the variable-phase mode converter, Opt. Commun. **181**, 35 (2000).
[26] T. Ohtomo, S.-C. Chu, and K. Otsuka, Generation of vortex beams from lasers with controlled Hermite- and Ince-Gaussian modes, Opt. Express **16**, 5082 (2008).
[27] S.-C. Chu and K. Otsuka, Stable donutlike vortex beam generation from lasers with controlled Ince-Gaussian modes, Appl. Opt. **46**, 7709 (2007).
[28] H. Laabs and A. T. Friberg, Nonparaxial eigenmodes of stable resonators, IEEE J. Quantum Electron. **35**, 198 (1999).
[29] S. Ngcobo, K. Aït-Ameur, N. Passilly, A. Hasnaoui, and A. Forbes, Exciting higher-order radial Laguerre–Gaussian modes in a diode-pumped solid-state laser resonator, Appl. Opt. **52**, 2093 (2013).
[30] M. A. Bandres and J. C. Gutiérrez-Vega, Ince–Gaussian modes of the paraxial wave equation and stable resonators, J. Opt. Soc. Am. A **21**, 873 (2004).
[31] B. Brecht, A. Eckstein, A. Christ, H. Suche, and C. Silberhorn, From quantum pulse gate to quantum pulse shaper—Engineered frequency conversion in nonlinear optical waveguides, New J. Phys. **13**, 065029 (2011).
[32] P. Manurkar, N. Jain, P. Kumar, and G. S. J. Kanterl, Programmable optical waveform reshaping on a picosecond timescale, Opt. Lett. **42**, 951 (2017).
[33] D. V. Reddy and M. G. J. Raymer, Photonic temporal-mode multiplexing by quantum frequency conversion in a dichroic-finesse cavity, Opt. Express **26**, 28091 (2018).
[34] V. Ansari, J. M. Donohue, M. Allgaier, L. Sansoni, B. Brecht, J. Roslund, N. Treps, G. Harder, and C. J. Silberhorn, Tomography and Purification of the Temporal-Mode Structure of Quantum Light, Phys. Rev. Lett. **120**, 213601 (2018).
[35] B. Brecht, D. V. Reddy, C. Silberhorn, and M. G. Raymer, Photon Temporal Modes: A Complete Framework for Quantum Information Science, Phys. Rev. X **5**, 041017 (2015).
[36] B. Sephton, A. Vallés, F. Steinlechner, T. Konrad, J. P. Torres, F. S. Roux, and A. J. Forbes, Spatial mode detection by frequency upconversion, Opt. Lett. **44**, 586 (2019).
[37] Y. R. Shen, *The Principles of Nonlinear Optics* (Wiley-Interscience, New York, 1984).
[38] G. B. Alves, R. F. Barros, D. S. Tasca, C. E. R. Souza, and A. Z. Khoury, Conditions for optical parametric oscillation with a structured light pump, Phys. Rev. A **98**, 063825 (2018).
[39] C. Hsueh and A. Sawchuk, Computer-generated double-phase holograms, Appl. Opt. **17**, 3874 (1978).
[40] O. Mendoza-Yero, G. Mínguez-Vega, and J. Lancis, Encoding complex fields by using a phase-only optical element, Opt. Lett. **39**, 1740 (2014).
[41] I. Kimel and L. R. Elias, Relations between Hermite and Laguerre Gaussian modes, IEEE J. Quantum Electron. **29**, 2562 (1993).
[42] P. Vaity, J. Banerji, and R. Singh, Measuring the topological charge of an optical vortex by using a tilted convex lens, Phys. Lett. A **377**, 1154 (2013).
[43] J. C. Lagarias, J. A. Reeds, M. H. Wright, and P. E. Wright, Convergence properties of the Nelder–Mead simplex method in low dimensions, SIAM J. Optim. **9**, 112 (1998).
[44] C. G. Broyden, The Convergence of a class of double-rank minimization algorithms 1. General considerations, IMA J. Appl. Math. **6**, 76 (1970).